Numerical analysis of the relationship between time-variant coda-Q and the variation in crustal stress

Kyosuke Okamoto, Hitoshi Mikada, Tada-nori Goto and Junichi Takekawa

Department of Civil and Earth Resources Engineering, Kyoto University, Kyoto 615-8540, Japan. E-mail: okamoto@tansa.kumst.kyoto-u.ac.jp

SUMMARY

Coda-Q is a stochastic parameter reflecting the heterogeneities of medium that seismic waves travel through. We confirmed that coda-Q would vary with the stress loaded to an elastic medium using numerical simulations of seismic wave propagation. When the stress is loaded, cracks in the crust could either close or newly open. The closure and opening of the cracks are not random but depending on the magnitude and the direction of the stress and the crack aspect ratio. The cracks in the medium after loading stress could be aligned in a specific orientation, and elastic wave velocity field would become anisotropic due to the alignment of specific crack orientations. Elastic wave velocity is in general faster along the direction corresponding with the crack orientation while slower along the perpendicular direction. In the numerical simulation, the effect of anisotropy in elastic wave velocity field due to the selective closure and opening of the cracks is calculated using a 2-D finite difference method assuming elastic wave velocity to be a function of the magnitude of loaded stress. The coda-Q calculated from seismic waves simulated for a model varies when the averaged normal stress changes. Our simulation indicated that the sensitivity of coda-Q^{-1}, that is the reciprocal of the coda-Q, would be 1.0×10^{-2} ($1.0 \, \text{MPa}^{-1}$) against the magnitude of the confining pressure and 1.0×10^{-3} ($1.0 \, \text{deg}^{-1}$) against the direction of principal stress. We would like to conclude that coda-Q, a stochastic parameter reflecting heterogeneities of subsurface medium, could become a quantitative state indicator of the stress field of the medium where seismic waves propagate through. Spatiotemporal variation of coda-Q reflects change in the stress field in the crust.

Key words: Seismic anisotropy; Seismic attenuation; Wave scattering and diffraction; Wave propagation.

1 INTRODUCTION

In earthquake studies, it is important to monitor change in the crustal stress field where earthquakes are generated. A stress field in the subsurface has been estimated using the stress relief experiment to sampled cores or boreholes, strainmeters buried in the subsurface, and electro distance meters (EDM), geodetic GPS measurement, etc. on the surface. In these techniques, the stress field is either indirectly estimated using the stress–strain relationship or directly obtained after releasing the loaded stress of the underground medium after costly construction of tunnels or drilling. However it is difficult to measure the stress at seismogenic depth because of the limitation of geodetic sensors, the cost of drilling, etc. Sano *et al.* (2004) pointed out that the measurement of the deep stress field is still a challenge with the present technologies, although information of the stress field at seismogenic depth is essential for further discussion of earthquake generation mechanisms. Recently, Hiramatsu *et al.* (2010) proposed that coda-Q (denoted as Q_c, hereafter) would be a parameter of the differential strain rate representing the spatial

variation of stress accumulation rate from the observation of Q_c in the vicinity of the 1995 Southern Hyogo Prefecture earthquake before and after the main shock event. Sugaya *et al.* (2009) discussed a change in Q_c after the 1995 Southern Hyogo Prefecture earthquake in connection with a property change in the crust, particularly in the lower crust. The cracks opened or closed by the stress change are one of the factors, which change the property of the crust. Jin *et al.* (2004) and Aki (2004) proposed a 'Brittle–Ductile Hypothesis' after finding a relationship between the variation of Q_c and the fractional frequency $N(M_c)$ of regional earthquakes with a certain magnitude range M_c from a long-term observation of the seismicity around the San Andreas Fault. The correlation coefficient between these two parameters became higher than 0.8.

The parameter Q_c is derived from the energy of a coda wave that decays exponentially with time (Fig. 1) caused by seismic scattering and friction due to inhomogeneities of the medium that the wave travels through. In practice, Q_c is obtained using coda envelope. We use Q_c in general as a stochastic parameter to represent the order of the inhomogeneities of the medium. Some papers
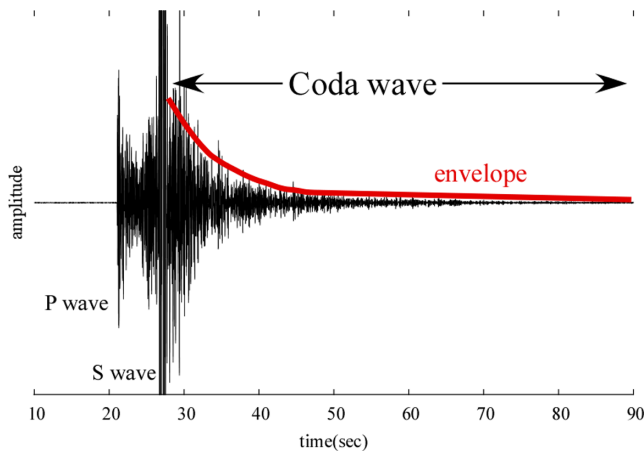
Figure 1. Later portion of a seismogram is a coda wave. Coda-*Q* is derived from attenuation ratio of the coda wave.

reported anomalous values of Q_c around volcanoes, faults (Jin & Aki 1988; Matsumoto & Hasegawa 1989; Got *et al.* 1990), which means the media has anomalous inhomogeneity. Also the recent results (Hiramatsu *et al.* 2000; Aki 2004) reported that the anomalous value of Q_c was detected after large earthquakes. These results indicate that the order of inhomogeneities may vary in the course of long-term earthquake generation cycle, that is, before and after the failure of crustal material takes place. Here we make a reasonable deduction with fair certainty that the stochastic parameter Q_c might have a certain relationship with physical or state properties of the stress field in the crust where seismic waves propagate through, since the change in the stress filed is a trigger of earthquakes. We therefore hypothesize that the state of stress acting in the subsurface medium could be estimated in the course of 'routine' seismic observation. No special observations or measurements would be necessary to acquire Q_c. If our hypothesis has been justified, we could propose that the monitoring of subsurface stress accumulation process is possible using the measurements of Q_c.

In this paper, we employ numerical simulation schemes to test our hypothesis that Q_c would vary with change in the stress acting on the medium where seismic waves travel through. Okamoto *et al.* (2010) examined the effect of elastic displacement of the cracks induced by the loaded stress on Q_c and concluded that the displacement might not be the major cause of Q_c change. Therefore, our hypothesis needs to be justified for the other causes that could change Q_c. We focus on selective closure and opening of the cracks when the stress is loaded. It makes the medium loaded to the stress anisotropic. Okamoto *et al.* (2011) discussed about effects of anisotropy in elastic wave velocity field using a point explosive source located in a centre of a model. Here anisotropy of elastic wave velocity field could occur due to selective closure and opening of microcracks (Nur 1971). And they pointed out that the effect of anisotropy of elastic wave velocity filed is one of major causes affecting Q_c. This time, we employ a plane wave as the incident wave and make detailed examinations of Q_c, for example, relationship with confining pressure, direction of the principal stress, etc. To simulate that the anisotropy on elastic velocity filed macroscopically, a 2-D finite difference method (FDM) is employed to calculate wave propagation in an anisotropic velocity field. Point scatterers are accommodated in the FDM model. At each scatterer, an incident wave is scattered and subsequently a coda wave is formed as a result of the superposition of the scattered waves. Also we consider microcracks distributed in the model having both the orientation angle

and the aspect ratio uniquely. The microcracks cannot be described with finite volume because the size is too small comparing with the grid size of the FDM. However the cracks change the model parameter conditions (i.e. compliance of the model) according with loaded stress and make the elastic velocity filed anisotropic.

2 THEORY

It is explained here how Q_c is obtained from a synthetic seismogram. Q_c is derived from a coda wave as mentioned in the introduction (Fig. 1). When the envelope of the coda wave $e(t)$ is assumed by eq. (1), Q_c is obtained as a part of the attenuation parameter.

$$\mathrm{e}(t) = A_0 t^{-n} \exp\left(-\frac{\pi f}{Q_c} t\right), \tag{1}$$

where A_0 is initial amplitude, t the time from a reference time when the wave passes by a certain reference point and f frequency. The term of t^{-n} represents the geometrical spreading. Power n is from 1 to 2 depending on the dominance wave, that is, surface, diffusive or body waves, in practice for a spherically emanating wave (Sato & Fehler 1997). However in this study we set $n = 0$ because of the assumption that the incident wave is a plane wave. To fit the envelope (eq. 1), several steps of data processing are applied to the coda wave. At first the Butterworth bandpass filter, whose band range is 8–16 Hz, is applied to a synthetic seismic wave. Then the Hilbert transform is applied to the bandpassed seismogram to fill intervals of the wave. In next step, the seismogram is smoothed using a rms technique (Roecker *et al.* 1982; Zelt *et al.* 1999; Kumar *et al.* 2005). Then this seismogram is taken the logarithm and eq. (2) is fitted using the least-square method. Fig. 2 shows the seismograms applied the procedures mentioned above.

$$\log \mathrm{e}(t) = -\frac{\pi f}{Q_c} t + \log A_0. \tag{2}$$

It is well known that Q_c is a function of frequency (e.g. Wu 1982), and the envelope of the coda wave would also be a function of frequency. However, we use a Ricker wavelet that peaks at a frequency of 15 Hz and a Butterworth filter of a passband of 8–16 Hz is applied before the estimation of Q_c in our study. The dependency of eqs (1) and (2) on the frequency could then be approximated by a constant value for a single frequency in the middle of such a narrow frequency range under the stationary phase approximation of the Fourier integral of waveforms. Therefore, we fix the frequency in eqs (1) and (2) to 12 Hz. Twice the traveltime of the incident wave has been used empirically as the initial time to fit eq. (2) (Aki & Chouet 1975; Rautian & Khalturin 1978). Because the early portion of coda wave is largely affected by a source function, fault direction, etc., twice the traveltime has been used as the initial time of a coda time window to avoid these effects. However in this study, we use same seismic source for all cases. So it is better to use longer time window for the coda wave to stabilize the estimation of Q_c^{-1} rather than shorten the coda time window using twice the traveltime as initial time of the coda time window. So we set 1.5 times the traveltime as the initial time of the coda time window. Still, here remains the problem that we cannot determine the origin time of the seismic source since we employ the plane wave coming from afar as the incident wave. So that, the traveltime is defined as the time during the plane wave propagates through from a side frame of the model to a receiver (Yomogida & Benites 1995). The receiver is located near from centre of the model in our study. The finish time of the coda time window is after 6.5 (s) from the origin time of the seismic source. We define the time window as mentioned
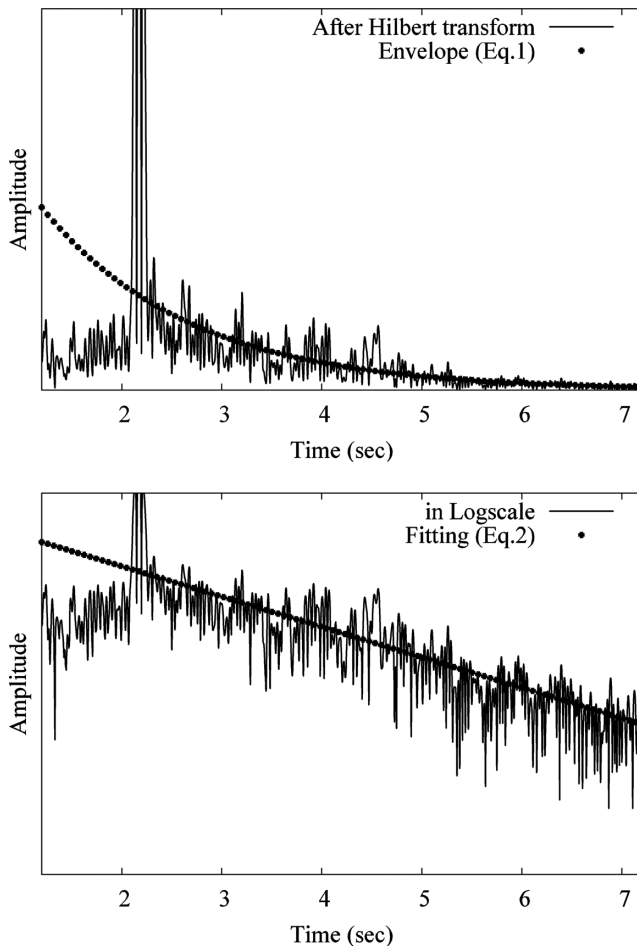
Figure 2. (a) The Hilbert transform is applied to a synthesized seismogram to fill intervals of the data. Eq. (1) is fitted to the seismogram as shown by the dotted line. (b) Practically eq. (2) is fitted to the seismogram in log-scale using least-square method. Then we can obtain the value of parameters in eq. (1).

above, however, commonly it is said that the early portion and the later portion of a seismogram reflect different character of attenuation. The early portion is dominated by the direct wave while the later portion is dominated by multiple scattering. So that various time windows having different initial and finish time, or different time length give different value of Q_c (e.g. in practice, Kosuga 1992 and in numerical simulation, Hoshiba 1991). So it is worth remarking that lapse-time dependence of Q_c is one of the most important issue to clarify. Also, it is another remained issue that which types of attenuation affects to Q_c dominantly, scattering or intrinsic attenuation. Many studies have been made to solve this problem (e.g. Wu 1985), however this issue is still under controversy. In this study we do not introduce intrinsic attenuation to the numerical simulations, so that, Q_c is contributed only by scattering attenuation.

3 VELOCITY ANISOTROPY

3.1 Theory

To simulate wave propagation using the FDM, the equation of motion for *SH* wave (eq. 3) and the stress–strain equation (eqs 4 and
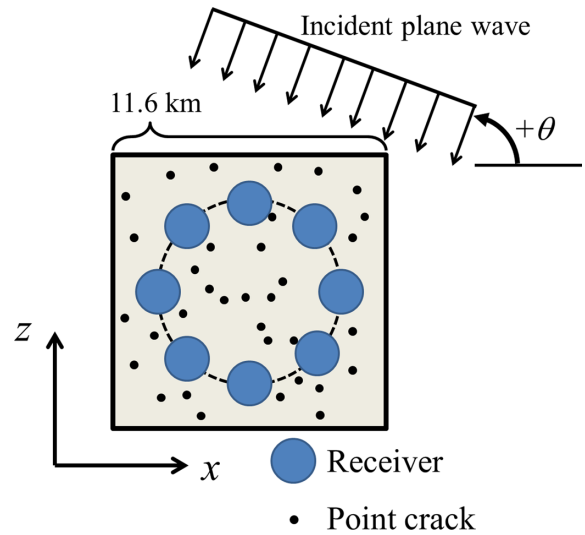

Figure 3. The model for the case of velocity anisotropy. This model includes the point shaped cracks, the fictitious cracks which only have information of orientation angle and aspect ratio, and the receivers. The point cracks scatter the incident wave while the fictitious cracks affect to elastic velocity.

5) are used as governing equations.

$$\rho \frac{\partial^2 u_y}{\partial t^2} = \frac{\partial \tau_{xy}}{\partial x} + \frac{\partial \tau_{yz}}{\partial z} \tag{3}$$

$$\tau_{xy} = \mu \frac{\partial u_y}{\partial x} \tag{4}$$

$$\tau_{yz} = \mu \frac{\partial u_y}{\partial z}, \tag{5}$$

where ρ is density, u is displacement, τ is shear stress, μ is the Lame's constant and x, y and z are spatial coordinates. These equations are discretized by the staggered grid (Virieux 1986; Levander 1988). Spatial accuracy is fourth-order and temporal accuracy is second-order. Eq. (6) should be satisfied to calculate stably.

$$0 < v \frac{\Delta t}{\Delta a} < \frac{1}{\sqrt{2}}, \tag{6}$$

where v is elastic wave velocity and Δt and Δa is temporal and spatial intervals, respectively. Here we set $\Delta t = 1.0 \times 10^{-3}$ (s) and $\Delta a = 11.6$ (m).

Fig. 3 shows the simulation model. Size of the model and time step are 1000×1000 grids and 8192 time steps, respectively. So, the model size is 11.6 (km) $\times$ 11.6 (km) and simulation time is 8.2 (s). Receivers are located circularly and incident wave comes from arbitrary angle θ (we use 0, 90, 180 and 270 as θ). The initial Young's module E and *S*-wave velocity V_s are 68.0 GPa and 3.5 km s^{-1}, respectively. Density of the model is 2.3 g cm^{-3}. The incident wave is the Ricker wavelet (eq. 7) whose centre frequency v_M is 15 Hz.

$$f(t) = \left(1 - 2\pi^2 v_M^2 t^2\right) \exp\left(-\pi^2 v_M^2 t^2\right). \tag{7}$$

Absorption boundary (Cerjan 1985) is introduced within 40 grids from the model frame. Within the absorption boundary amplitude of the synthetic wave $A(j)$ decreases according to eq. (8). Amplitude at jth grid becomes $A(j) \times G(j)$.

$$G(j) = \exp[-\varepsilon (40 - j)^2]. \tag{8}$$

The amplitude of reflected waves from the absorption boundary becomes only 0.1 per cent of that of the incident waves and when
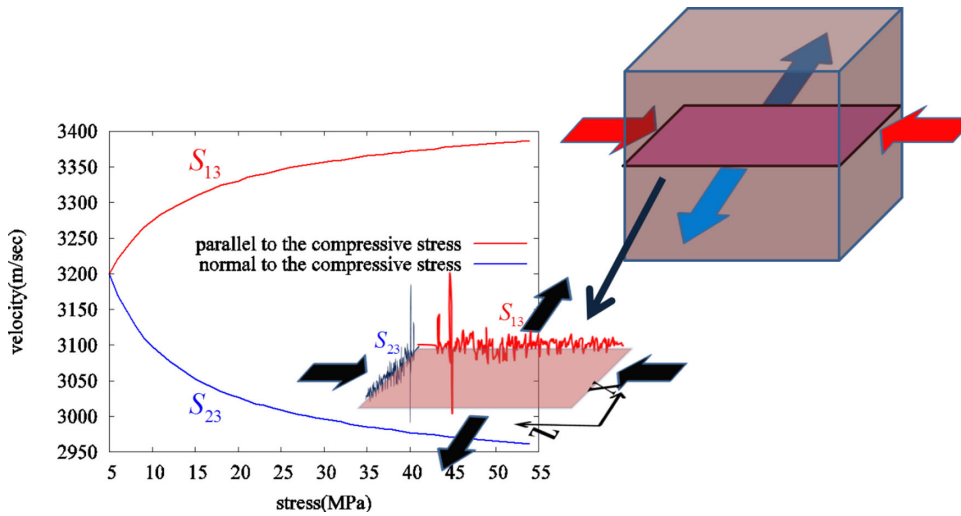
Figure 4. The pure shear stress opens or closes microcracks and velocity anisotropy occurs. The velocity along the compressive stress S_{13} increases due to closure of the cracks and the velocity along the tensile stress S_{23} decreases due to opening of the cracks.

we set ε to 8.0×10^{-3}. Also the averaged amplitude of the reflected is 3 per cent of that of the scattered waves in the coda time window. These observations indicate that the absorption boundary attenuates enough to make the reflected negligible.

To this model 5000 scatterers are distributed at random position and their shape is described as point. The set of shear stress shown in eqs (3) to (5) is zero at the scatteres. A point shaped scatterer scatters the incident wave and the waves scattered from the other scatterers isotropically. The superposition of the scattered waves forms a coda wave. The point shaped scatterers are not affected by loading stress, which means they remain initial condition during the loading.

Aside from these point shaped scaterers, we assume 5000 microcracks having aspect ratio α (ratio of minor and major radius) and orientation angle φ as parameter. These microcracks do not have finite volume because the size is too small comparing with the grid size and they are used only for calculating S-wave velocity at the given stress. $N(\alpha)$ in eq. (9) is fractional number of the fictitious cracks whose aspect ratio is α. The number of cracks decreases proportionally as aspect ratio α increases.

$$N(\alpha) = N_0 \left(1 - \frac{\alpha}{\alpha_m}\right) \quad \alpha \leq \alpha_m$$
$$N(\alpha) = 0 \quad \alpha > \alpha_m \tag{9}$$

where N_0 and α_m are constants. We took $a_m = 5.0 \times 10^{-4}$, which value is same as Nur (1971). Here we assume that cracks which satisfy eq. (10) are closed due to the compressive stress. If the loaded stress is tension, cracks satisfying eq. (11) are newly opened. The number of the newly opened cracks is same as the number of the closed crack when the same magnitude of the compressive stress is loaded. This selective closure and opening make the elastic velocity field anisotropic. These assumptions are same as that of Nur (1971).

$$\alpha \leq \frac{\sigma_n}{E} \tag{10}$$

$$\alpha > \frac{\sigma_n}{E}, \tag{11}$$

where σ_n is component of the loaded stress normal to a crack.

The compliance tensor when stress σ is loaded, $S(\sigma)$, can be calculated as a function of $N(\alpha)$ and σ according to Nur (1971). Then, we can calculate the S-wave velocities along x- and z-axes when the

stress σ is loaded. We use these values as the S-wave velocity of the model. Fig. 4 shows variation of the elastic velocities along the x- and z-axes when the compressive and tensile stresses are loaded perpendicularly at the same magnitude (pure shear stress). The variation of velocity is controlled partly by distribution of crack aspect ratio. If α_m in eq. (9) is larger, velocity changes more significantly. It is because closure of a larger crack makes bigger variation in elastic velocity.

While S-wave velocity is changed according with the loaded stress, we assume that the point shaped scatterers are remain as same as original condition. It means that the incident wave is scattered as frequent as the initial model even after S-wave velocity is changed. We can examine the effect of change in elastic wave velocity field without change in number density of the scatterers and scattering pattern at each scatterer.

In practice compressive, tensile or pure shear stress is loaded to the model shown in the Fig. 3. Fig. 5 shows three loading patterns, the reverse, normal and strike case. In the reverse case, in which compressive stress is loaded, the confining pressure s (eq. 12) is always positive and magnitude of the confining pressure increases as magnitude of the stress increases.

$$s = \frac{(\sigma_x + \sigma_z)}{2}. \tag{12}$$

In the normal case, in which tensile stress is loaded, the confining pressure is always negative and magnitude of the confining pressure decreases as magnitude of the stress increases. In the strike case, compressive and tensile stresses are loaded at the same magnitude perpendicularly, so the confining pressure becomes zero by cancelling each other out. In the numerical experiment magnitude
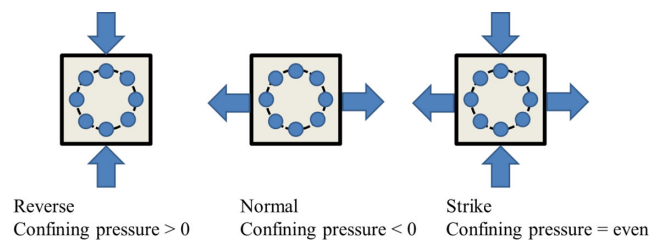

| Reverse | Normal | Strike |
| Confining pressure > 0 | Confining pressure < 0 | Confining pressure = even |

Figure 5. Three different loading patterns. We call the patterns as reverse, normal and strike cases from left to right, respectively.

of the stress is changed from 5 to 50 MPa. Q_c^{-1} is estimated at each receiver location. After the estimation of Q_c^{-1} at eight receiver locations as shown in Fig. 3, the average value of Q_c^{-1}, that is, what we call averaged Q_c^{-1}, is estimated over all the receivers for a given incident angle. Since there is another parameter called the incident angle of seismic waves coming into the model, we take the azimuthal average of the averaged Q_c^{-1} values for four different incident angles perpendicular to each other surrounding the model. The azimuthal average is called as the stacked Q_c^{-1} that is free from any influence due to the observation location in the model and to the difference in the incident angle of seismic waves.

3.2 Result

Fig. 6 shows result of the FDM. The stacked Q_c^{-1} is plotted against the magnitude of the loaded stress. In the reverse case, in which the confining pressure increases, the stacked Q_c^{-1} also increases. Also in the normal case the stacked Q_c^{-1} has relationship with the confining pressure. Smaller the confining pressure is, lower the value of the stacked Q_c^{-1} marks. The stacked Q_c^{-1} shows minor fluctuation against the stress in the strike case. This change in the stacked Q_c^{-1} against the loaded stress is due to change in the elastic velocity field (Okamoto *et al.* 2011). In the reverse case the compressive stress closes the cracks satisfying eq. (10) and the elastic velocity increases. In the normal case the tensile stress newly opens cracks and the elastic velocity decreases. On the other hand, in the strike case the compressive stress, loaded along the *x*-axis, closes cracks and the tensile stress, loaded along the *z*-axis, newly opens cracks by the same number as the cracks closed by the compressive stress. Consequently the velocity along the *x*- and *z*-axes increases and decreases, respectively as shown in Fig. 4. These two opposite effects superpose each other and the stacked Q_c^{-1} would not show any change against the magnitude of the stress in the strike case. In the reverse and the normal cases, the change in the velocity could not be cancelled out in terms of the confining pressure, and the stacked Q_c^{-1} varies with the magnitude of the stress. If the magnitudes of the two perpendicular horizontal stresses in the strike case cause the confining pressure to vary, the stacked Q_c^{-1} could show a similar tendency in the change against the magnitude of the stress as in the other normal or reverse cases. It could be summarized that the stacked Q_c^{-1} varies with the confining pressure *s* in eq. (12). Fig. 7 shows change in formation of the coda wave when the velocity increases. When the velocity increases, each phase of the scatter
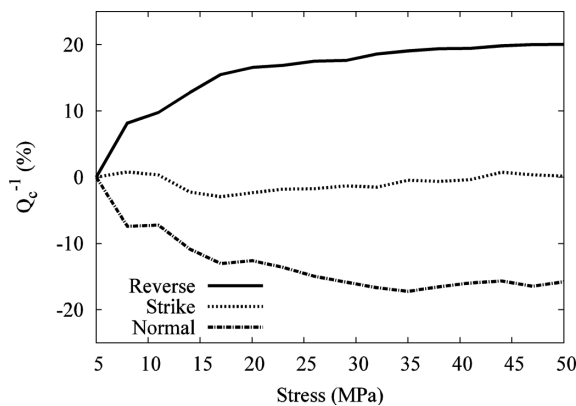

Figure 6. The stacked Q_c^{-1} is plotted against magnitude of the stress. The results of the three patterns (the reverse, the normal and the strike cases) are shown.
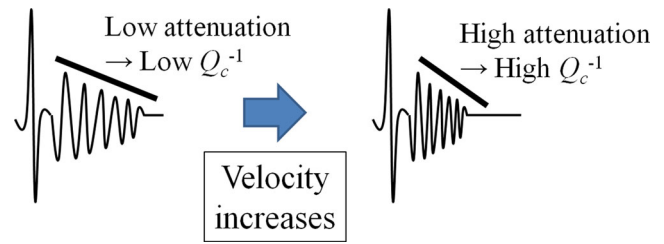

Figure 7. Shape of the coda wave is changed due to change in the elastic velocity. The coda wave attenuates rapidly, and then Q_c^{-1} increases when elastic velocity increases.
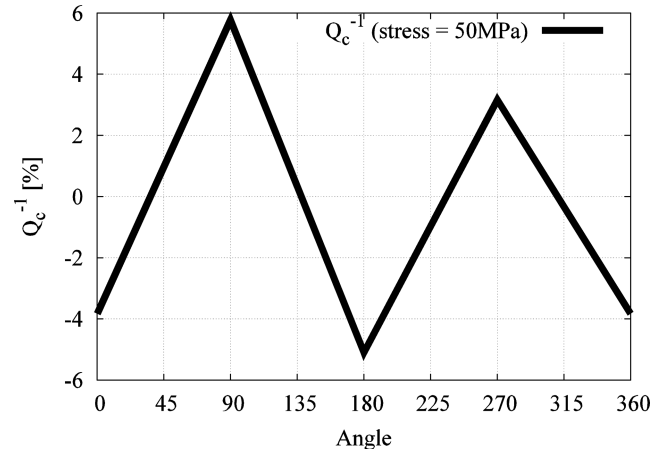

Figure 8. The averaged Q_c^{-1} is plotted against angle of the principal stress.

waves reaches the receiver much rapidly. Thus the coda wave attenuates rapidly. It leads to higher attenuation ratio, therefore the stacked Q_c^{-1} marks higher value (see eq. 1).

Next directional dependence of the averaged Q_c^{-1} (not the stacked Q_c^{-1}) is examined. Direction of the stress is rotated, with location of the receivers, angle of incident wave and magnitude of the stress (50 MPa) fixed. The pure stress is loaded; normal stress is loaded along *x*-axis and compressive stress is loaded along *z*-axis at the same magnitude. As a result, the averaged Q_c^{-1} varies periodically in accordance with direction of the principal stress (Fig. 8). The averaged Q_c^{-1} marks the maximum value when direction of the principal stress coincides with direction of the incident wave. On the other hand the averaged Q_c^{-1} marks the minimum value when the direction of the principal stress is perpendicular to the direction of the incident wave. This variation of the averaged Q_c^{-1} can be explained by the anisotropy in the elastic velocity filed. Since the velocity along the principal stress (S_{13} in Fig. 4) is higher than the velocity along other directions, the averaged Q_c^{-1} marks the maximum value at the direction parallel to the principal stress. On the other hand, the averaged Q_c^{-1} marks the minimum value due to the low velocity when direction of the principal stress is perpendicular to direction of the incident wave.

4 DISCUSSIONS

We have considered the effect of anisotropy of elastic wave velocity field that could influence Q_c^{-1}. The effects of the change in the confining pressure and the direction of the principal stress on Q_c^{-1} were examined for an anisotropic medium. Following Hiramatsu *et al.*

(2010), we define the sensitivity of the Q_c^{-1} against the magnitude and the direction of the stress by eq. (13)

$$\left| \frac{1}{Q_c^{-1}} \frac{dQ_c^{-1}}{d\sigma} \right| \quad \text{(magnitude)}$$

$$\left| \frac{1}{Q_c^{-1}} \frac{dQ_c^{-1}}{d\theta} \right| \quad \text{(angle)}$$

(13)

The sensitivity of the change in the averaged Q_c^{-1} is about 1.0×10^{-3} (1 deg^{-1}) against the direction of the principal stress. The stacked Q_c^{-1} is calculated by geometric or azimuthal average of the averaged Q_c^{-1} on a closed surface surrounding the medium. The stacked Q_c^{-1} does not therefore have any directional dependence. When the velocity anisotropy is considered, the sensitivity of the stacked Q_c^{-1} against the magnitude of the confining pressure is at most about 1.0×10^{-2} (1 MPa^{-1}). The sensitivity peaks approximately at the low magnitude of the stress. At the high magnitude of the stress, the sensitivity becomes almost negligible. Here we notice that the sensitivity of the Q_c^{-1} against the stress is approximately small compared to that found by Hiramatsu *et al.* (2010), which is 10 (1 MPa^{-1}). This is because we made some assumptions on the initial distribution of crack aspect ratio α_m, the number density of the cracks, etc. They would not change the trend of the Q_c^{-1} against the loaded stress, that is, whether the value increases or decreases, because this trend depends not on the initial condition of the cracks but on the closure or the opening of the cracks when the stress is loaded. However the magnitude of the variation of the Q_c^{-1} should change with the different initial conditions of the cracks. Also, $\delta Q_c^{-1}/Q_c^{-1}$ could become smaller value than that of Hiramatsu *et al.* (2010). Here the δQ_c^{-1} is the difference between the current value of Q_c^{-1} and the previous value of Q_c^{-1}. The value of $\delta Q_c^{-1}/Q_c^{-1}$ is 6.0×10^{-4} when the stress is loaded with the rate of 13 kPa yr^{-1} for 2 yr, while the value of $\delta Q_c^{-1}/Q_c^{-1}$ in Hiramatsu *et al.* (2010) about 2.7×10^{-1}. The discrepancy would be also due to the difference between the initial condition of the simulation model and the real conditions in the field data.

It has been known that value of the Q_c changes before and after an earthquake or during a preparation period for a next earthquake. However the trend of the variation of Q_c^{-1} has not been well discussed. Q_c increases in some cases and decreases in other cases (Sato 2003). This is partly because the Q_c is analysed without considering on the relationship among the orientation of the incident wave, the principal stress, and the change in the confining pressure, etc. (Sato 1988). When we analyse data to acquire change in the stress field in the subsurface in practice, we should pay attention to the geometry of receivers and hypocenters since the difference in the orientation of the incident wave propagation could give different values of the Q_c^{-1}. From the change in the observed Q_c^{-1}, the variation in the magnitude of the confining pressure can be acquired as shown in the flow chart (Fig. 9) if direction of the principal stress is fixed. We could eliminate the azimuthal dependence of the Q_c^{-1}, considering the orientation of the incident wave propagation, and then, could look at the Q_c^{-1} variation with respect to the magnitude of the confining pressure. As one of the other means to eliminate orientation dependence of the Q_c^{-1}, we average the estimated Q_c^{-1} over the earthquakes that surround the medium of interest.

In Japan, the amount of the stress drop after major damaging earthquakes is at most 10 MPa for shallow intraplate earthquakes, and 100 MPa for the earthquakes near the subduction zones. The change in the confining pressure of several MPa is equivalent to that of 10^{-2}–10^{-1} in the stacked Q_c^{-1} according to our results. Londono (1996) observed the Q_c^{-1} with an error of about
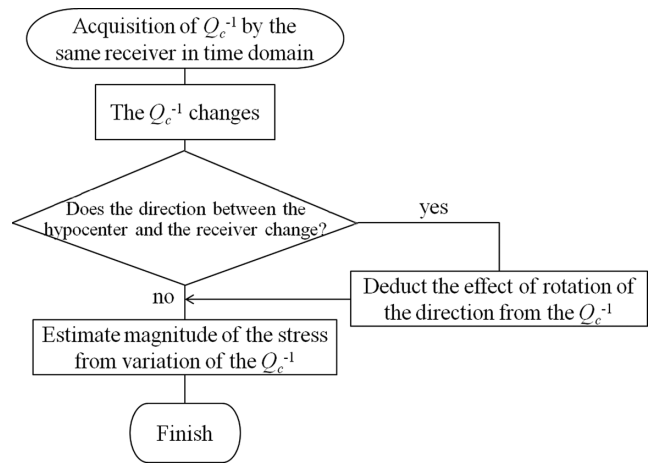

Figure 9. The flow chart to obtain magnitude of the stress from the observed Q_c^{-1}. It is assumed that direction of the principal stress does not change.

10^{-3}–10^{-4}. Therefore, we think it is possible to detect the stress variation before or after an earthquake from observation of the Q_c^{-1}.

When we apply the method to real data, we should remind that only the scattering attenuation has been under consideration in the numerical studies. Real data may also suffer from the influence of the intrinsic attenuation of the medium, and it could be necessary to deal with the intrinsic Q. Some studies have reported that the intrinsic attenuation could be negligible (i.e. Margerin *et al.* 1999), while some other studies have reported that the scattering is comparable or smaller than intrinsic attenuation (i.e. Hoshiba *et al.* 2001). Since we are focusing our discussions on the change of Q_c^{-1}, we might be able to ignore the influence of the intrinsic Q based on the assumption that the intrinsic Q is not so sensitive to the change of stress field. Our results are based on the intrinsic attenuation is negligible. Some methods such as the multiple lapse time window analysis, developed by Fehler *et al.* (1992), separate the effect of the intrinsic and the scattering attenuation.

5 CONCLUSIONS

In this study, we first hypothesized that there is a certain relationship between change in the stress field in the subsurface and value of Q_c^{-1}. Although the displacement in the crack locations due to loaded stress could induce the minor change in Q_c^{-1}, there should be other causes, such as the effects of velocity anisotropy, affecting to Q_c^{-1} more effectively than the effect of elastic displacement of the crack location. When the stress is loaded, the crack having particular orientation angle and aspect ratio is closed or newly opened. Due to this opening and closing, elastic wave velocity changes and shape of the coda wave also changes. Therefore value of Q_c^{-1} is also changed. In other words, value of the Q_c^{-1} is changed because loaded stress changes condition of the cracks in the crust. We examined how the change in the crack condition affects to the value of the Q_c^{-1} using the numerical simulation. As the results, it has become clear that the change in the Q_c^{-1} has a relationship with change in the stress field, concretely magnitude and principal direction of the stress. More precisely, the change in the Q_c^{-1} has a proportional relationship with change in magnitude of the confining pressure and direction of the principal stress. The sensitivity is 1.0×10^{-2} (1 MPa^{-1}) for

the case when magnitude is changed and 1.0×10^{-3} (1 deg^{-1}) for the case when direction is changed.

We assumed several assumptions in our study; intrinsic attenuation is negligible comparing with scattering attenuation, plane wave coming from arbitrary direction can be used, etc. When we examine if the relationship between Q_c^{-1} and the crustal stress, which we have revealed in the numerical studies, exists in real data, we need to pay attention to the assumptions.

REFERENCES

Aki, K., 2004. A new view of earthquake and volcano precursors, *Earth Planets Space,* **56,** 689–713.

Aki, K. & Chouet, B., 1975. Origin of coda waves: source, attenuation, and scattering effects, *J. geophys. Res.,* **80,** 3322–3342.

Cerjan, C., 1985. A nonreflecting boundary condition for discrete acoustic and elastic wave equations, *Geophysics,* **50,** 705–708.

Fehler, M., Hoshiba, M., Sato, H. & Obara, K., 1992. Separation of scattering and intrinsic attenuation for the Kanto-Tokai region, Japan, using measurements of S-wave energy versus hypocentral distance, *Geophys. J. Int.,* **108,** 787–800.

Got, J.L., Pouoinet, G. & Frechet, J., 1990. Changes in source and site effects compared to coda Q^{-1} temporal variations using microearthquakes doublets in California, *PAGEOPH.,* **134,** 195–228.

Hiramatsu, Y., Hayashi, N., Furumoto, N. & Katao, H., 2000. Temporal changes in coda Q^{-1} and *b* value due to the static stress changes with the 1995 Hyogo-ken Nanbu earthquake, *J. geophys. Res.,* **105,** 6141–6151.

Hiramatsu, Y., Iwatsuki, K., Ueyama, S. & Iida, T., 2010. Spatial variation in shear wave splitting of the upper crust in the zone of inland high strain rate, central Japan, *Earth Planets Space,* **62,** 675–684.

Hoshiba, M., 1991. Simulation of multiple-scattered coda wave excitation based on the energy conservation law, *Phys. Earth planet. Inter.,* **67,** 123–136.

Hoshiba, M., Rietbrock, A., Scherbaum, F., Nakahara, H. & Haberland, C., 2001. Scattering attenuation and intrinsic absorption using uniform and depth dependent model—application to full seismogram envelope recorded in Northern Chile, *J. Seismol.,* **5,** 157–179.

Jin, A. & Aki, K., 1988. Spatial and temporal correlation between coda Q and seismicity in China, *Bull. seism. Soc. Am.,* **78,** 741–769.

Jin, A., Aki, K., Liu, Z. & Keilis-Borok, V.I., 2004. Seismological evidence for the brittle-ductile interaction hypothesis on earthquake loading, *Earth Planets Space,* **56,** 823–830.

Kosuga, M., 1992. Dependence of coda Q on frequency and lapse time in the western Nagano region, central Japan, *J. Phys. Earth,* **40,** 421–445.

Kumar, N., Parvez, I.A. & Virk, H.S., 2005. Estimation of coda wave attenuation for NW Himalayan region using local earthquakes, *Phys. Earth planet. Inter.,* **151,** 243–258.

Levander, R., 1988. Fourth-order finite-difference P-SV seismograms, *Geophysics,* **53,** 1425–1436.

Londono, J.M., 1996. Tenporal change in coda Q at Nevado Del Ruiz Volcano, Colombia, *J. Volc. Geotherm. Res.,* **73,** 129–139.

Margerin, L., Cmpillo, M., Shapiro, N.M. & Tiggelen, B.V., 1999. Residence time of diffuse waves in the crust as a physical interpretation of coda Q: application to seismograms recorded in Mexico, *Geophys. J. Int.,* **138,** 343–352.

Matsumoto, S. & Hasegawa, A., 1989. Two-dimensional coda Q structure beneath Tohoku, NE Japan, *Geophys. J. Int.,* **99,** 101–108.

Nur, A., 1971. Effect of stress on velocity anisotropy in rocks with cracks, *J. geophys. Res.,* **76,** 2022–2034.

Okamoto, K., Mikada, H., Goto, T., Takekawa, J. & Onishi, K., 2010. Relation between coda-Q and stress loaded to an elastic body-parameters of material conditions derived by stochastic measurement: effect of elastic displacement-, *Explor. Geophys,* **63,** 519–529 [in Japanese with English abstract].

Okamoto, K., Mikada, H., Goto, T. & Takekawa, J., 2011. Numerical studies on stress field monitoring using coda-Q, *SEG Expand. Abs.,* **30,** 4229–4233.

Rautian, T.G. & Khalturin, V.I., 1978. The use of the coda for determination of the earthquake source spectrum, *Bull. seism. Soc. Am.,* **68,** 923–948.

Roecker, S.W., Tucker, B., King, J. & Hatzfeld, D., 1982. Estimation of Q in central Asia as a function of frequency and depth using the coda of locally recorded, *Bull. seism. Soc. Am.,* **72,** 129–149.

Sano, O., Ito, H. & Mizuta, Y., 2004. Present situation, problems and feature challenges in measurement of tectonic stress, *Chikyu Monthly,* **295,** 3 [in Japanese].

Sato, H., 1988. Temporal change in scattering and attenuation associated with the earthquake occurrence—a review of recent studies on coda eaves, *PAGEOPH,* **126,** 465–497.

Sato, H. & Fehler, M., 1997. *Seismic Wave Propagation and Scattering in the Heterogeneous Earth,* 1st edn, Springer, Berlin.

Sato, T., 2003. Relation of stress drops of small and moderate earthquakes to focal mechanism, fault type, focal depths, and regions, *J. Earthq. Eng.,* **27,** 211–219 [in Japanese with English abstract].

Sugaya, K., Hiramatsu, Y., Furumoto, M. & Katao, H., 2009. Coseismic change and recovery of scattering environment in the crust after the 1995 Hyogo-ken Nanbu Earthquake, Japan, *Bull. seism. Soc. Am.,* **99,** 435–440.

Virieux, J., 1986. P-SV wave propagation in heterogeneous media: velocity-stress finitedifference method, *Geophysics,* **51,** 889–901.

Wu, R.-S., 1982. Attenuation of short period seismic waves due to scattering, *Geophys. Res. Lett.,* **9,** 9–12.

Wu, R.-S., 1985. Multiple scattering and energy transfer of seismic waves-separation of scattering effect from intrinsic attenuation—I. Theoretical modeling, *Geophys. J. R. astr. Soc.,* **82,** 57–80.

Yomogida, K. & Benites, R., 1995. Relation between direct wave Q and coda Q: a numerical approach, *Geophys. J. Int.,* **123,** 471–483.

Zelt, B.C., Dotzev, N.T., Ellis, R.M. & Rogers, G.C., 1999. Coda Q in southwestern British Columbia, Canada, *Bull. seism. Soc. Am.,* **89,** 1083–1093.